

Abstract

The effect of hull dynamics in shallow water on the hydrodynamic performance of rowing shells and/or canoes and kayaks is investigated. An approach is developed to generate data in a towing tank using a test rig capable of reproducing realistic speed profiles. The impact of unsteady shallow-water effects on wave-making resistance is examined via experimental measurements on a benchmark hull.

The data generated has been used to explore the validity of a computational approach developed to predict unsteady shallow-water wave resistance.

Comparison of measured and predicted results show that the computational approach correctly predicts complex unsteady wave-resistance phenomena at low oscillation frequency and speed, but that total resistance is substantially under-predicted at moderate oscillation frequency and speed.

It is postulated that this discrepancy arises from unsteady viscous effects. This is investigated via hot-film measurements for a full-scale single scull in unsteady flow in both towing tank and field-trial conditions. Results suggest a strong link between acceleration and turbulence and demonstrate that the measured real-world viscous-flow behaviour can be successfully reproduced in the tank.

Thus it is shown that a suitable tank-test approach can provide a reliable guide to hull performance characterisation in unsteady flow.

1 Introduction

1.1 Background and literature review

In boat-based sports, sailing has long led the way in the application of physical testing, in test-tanks, wind tunnels and at full-scale, as well as computational analysis, driven especially by the high budgets of America's Cup yacht design. In rowing, canoeing and kayaking, the use of both computational hydrodynamics and physical testing in performance assessment has been more limited.

Steady-speed thin-ship (inviscid) computational studies of rowing shells were carried out by Tuck and Lazauskas (1996), and Lazauskas (1998). Scragg and Nelson (1993) used a steady-speed inviscid wave-resistance code, including shallow-water effects, to predict the performance and design two hulls. More recently Formaggia et. al. (2007, 2009), computed the effects of heave and pitch motions on resistance using a potential-flow approach, and later utilised this in a sophisticated dynamic model of the rower-hull-fluid system. Berton, Alessandrini, Barré, and Kobus (2007), presented results for an unsteady viscous Computational Fluid Dynamics (CFD) approach. Other studies (e.g. Wellicome (1967)) have utilised steady-speed tank tests as an aid to the development of improved hull-forms for rowing shells; many other tank-test studies carried out remain commercially confidential.

The application of these techniques to canoes and kayaks has been more limited. Lazauskas and Tuck (1996), applied the steady-speed thin-ship approach to explore optimal hull forms for racing kayaks; Lazauskas and Winters (1997) compared the performance of optimal hull-forms and some real designs. Bugalski (2009) documents the history of canoe hull-form development, and outlines a detailed

1
2
3 technical program implemented in support of the design of Plastex canoes, including
4 tank-testing and CFD applications.
5
6

7
8 As hull designs evolve, the available gains diminish, and increased demands are
9 placed upon the accuracy of both experimental and computational approaches.
10

11
12 Nonetheless, the extremely small winning margins still justify the extraction of every
13 last possible improvement. In the Beijing Olympics, over the fourteen rowing events,
14 eighteen crews were within 0.5% of mean speed of the gold medal-winning crews in
15 their event, from as low as fourth place, whilst thirty-three were within 1%.
16
17

18
19 Consequently, effects which might have previously been considered too small or too
20 challenging to model may need to be considered, even where inclusion of these
21 effects requires novel approaches. Two such effects are explored here: the impact
22 of shallow water, and effect of unsteady variation in speed through the stroke.
23
24
25
26
27
28
29

30 31 **1.2 Effect of water depth**

32
33 The key parameter in characterising the effect of water depth on resistance is the
34 *depth Froude Number*, $F_{rh} = U / \sqrt{gh}$ where U is boat speed, g is the gravitational
35 constant and h is water depth. If $F_{rh} \leq 0.5$, results are similar to deep water. As the
36 boat approaches the *critical* speed ($F_{rh} = 1.0$), wavelengths, wave heights and wave
37 resistance all increase. Indeed, for this reason, high-speed ferries normally avoid
38 operating in a depth Froude number range of 0.8-1.2. For *supercritical* ($F_{rh} > 1.0$)
39 speeds the transverse components of the wave pattern disappear and the wave
40 resistance may reduce compared to the critical value. Faltinsen (2005) gives a
41 detailed discussion of the effect of water depth on wave patterns and wave
42 resistance.
43
44
45
46
47
48
49
50
51
52
53
54
55
56

57
58 On a rowing lake with depth of 3.0m, the critical speed is around 5.4m/s; many elite
59 rowers will be travelling at this speed at some point in their stroke cycle. Hence it is
60

1
2
3 important to be able to account for the effects of shallow water both experimentally
4
5 and computationally in a first-principles approach to hull design.
6
7

8 **1.3 Effect of unsteady speed**

9
10 The surge acceleration of a rowing shell can be substantial. Figure 1, replotted from
11
12 Kleshnev (2002), shows acceleration for a men's rowing pair at a rate of 35
13
14 strokes/minute, plotted against a proportion of the stroke period $T = 1.71s$. The
15
16 maximum deceleration here is over 1g, occurring in the "catch" phase of the stroke.
17
18 Assuming a mean speed of 5.0m/s (equivalent to a medal time for a rowing pair in
19
20 Beijing), the associated speed variation and distance travelled can be found by time
21
22 integration. The range of the speed variation is almost 50% of the mean value; in
23
24 3.0m water depth, the depth Froude Number would vary from 0.65-1.09.
25
26
27

28
29 The speed variation modifies the resistance in two key ways. Firstly, the waves
30
31 generated by the boat, and the associated wave-making resistance, will change.
32
33 These changes will be more pronounced in shallow water, especially close to the
34
35 critical speed. Secondly the boundary layer around the hull will be affected, leading
36
37 to changes in the viscous resistance; these changes are less likely to be sensitive to
38
39 water depth.
40
41

42 **1.4 Aim and Objectives**

43
44 The current study aims to contribute to the understanding of the effect of unsteady
45
46 hull dynamics in shallow water on the wave-making and viscous resistance of
47
48 rowing shells, canoes and kayaks. It is intended to achieve this aim by developing
49
50 an experimental approach which can be shown to generate realistic physical test
51
52 data in laboratory conditions, and through the examination of a computational
53
54 approach to predict unsteady shallow-water wave resistance.
55
56

57
58 The objectives of the current study are:
59
60

- 1) to design and build a test rig capable of reproducing realistic speed profiles in the towing tank;
- 2) to use the rig to explore the impact of unsteady shallow-water effects on wave-making resistance via experimental measurements on a benchmark hull;
- 3) to use the data generated to explore the validity of a computational approach to the prediction of unsteady wave resistance;
- 4) to examine the impact of unsteady speed on viscous flow around the hull in real-world and laboratory conditions;
- 5) to demonstrate that the measured real-world viscous flow behaviour can be successfully reproduced in the tank and thus that a tank-test approach can provide a reliable guide to viscous-flow performance characterisation.

2 Development of test rig

The test rig was designed to be installed in the towing tank at the XXX Laboratory in XXX. The tank has dimensions 76.0×4.57×2.5m, with water depth of up to 2.3m.

Previous experiments had used the main towing carriage to generate unsteady motion; however the peak acceleration of the carriage (weighing over seven tonnes) is limited to around 0.8m/s^2 , or less than 10% of the peak value shown in Figure 1.

In the present study, the main towing carriage was used to generate the mean speed, and a sub-carriage was mounted on the main carriage to generate the surging motion. The specification of the sub-carriage required careful consideration of full-scale behaviour and appropriate similarity (scaling) conditions. The data from Figure 1 was used in the first instance to outline the specifications.

The requirements for a full-scale pair can be obtained by subtracting the mean speed, and the distance travelled at mean speed, from the corresponding

1
2
3 instantaneous values of speed and distance, to give the perturbation speed and the
4
5 excursion required for the sub-carriage, shown in Figure 2.
6
7

8
9 In order to scale wave effects correctly the Froude Number based on length,

10
11 $F_r = U/\sqrt{gL}$, is kept constant between model and full-scale. Here U is the speed
12
13 and L is waterline length. Under Froude scaling, accelerations are identical at
14
15 model and full scale; model-scale speed is reduced as the square-root of the scale
16
17 factor. For a rowing pair, with length 10.25m, mass 195kg, mean speed 5.0m/s, and
18
19 stroke rate of 35 strokes/min in a water depth of 3.0m, at a scale of 1:2, the model
20
21 would be 5.125m long, with mean speed 3.54m/s, stroke frequency of 0.82Hz, in
22
23 water of depth 1.5m.
24
25

26
27 After allowing for acceleration and deceleration of the main carriage, this would yield
28
29 around 10 cycles at a steady mean speed. However the total displacement of the
30
31 model would be only around 25kg, so a lightweight model hull would be required.
32
33

34 Using the data from Figure 2, the model-scale perturbation speed would vary from
35
36 -1.05 to +0.64m/s and the excursion from -0.12m to + 0.14m.
37
38

39 A digitally-controlled electrically-driven actuator available from a previous project,
40
41 with maximum travel of 1m, speed of 2m/s, acceleration of 20m/s², and force of
42
43 20kN was seen to be adequate. The actuator drives a sub-carriage approximately
44
45 2.0×1.0m on which the standard towing system is mounted (see Figure 3). Pre-
46
47 calculated data points specify carriage position at each moment in time through one
48
49 cycle; the cycle is repeated to generate periodic motion. The complete test set-up
50
51 for shallow water is shown in Figure 4.
52
53

54
55 Only the surging motion of the boat is controlled in the system. For rowing shells,
56
57 fore-and-aft movement of the athletes and the surging acceleration of the boat lead
58
59 to a pitching motion, whilst vertical acceleration of the athletes and oars leads to a
60

1
2
3 heaving motion. In the current system these motions are not controlled;
4
5 nonetheless, the boat can heave and pitch freely due to the varying hydrodynamic
6
7 forces.
8
9

10 Where the testing focus is on measurement of unsteady hydrodynamic forces,
11
12 inertial forces become extremely important. These are typically an order of
13
14 magnitude larger than the steady hydrodynamic forces, and possibly two orders of
15
16 magnitude larger than unsteady effects. Hence the force measurement system has
17
18 to be highly sensitive, linear, and repeatable, and both the acceleration and the hull
19
20 mass must be measured extremely precisely.
21
22
23
24
25

26 **3 Tank testing of benchmark hull in shallow water**

27
28 The first set of tank tests explored the effect of unsteady wave-making resistance in
29
30 shallow water, using the well-known benchmark design, the *Wigley* hull, which has
31
32 parabolic waterlines and sections. The model was constructed with length $L = 3.0\text{m}$,
33
34 beam $B = 0.3\text{m}$ and draught $T = 0.1875\text{m}$. The Wigley hull is less slender than a
35
36 rowing shell; however the increased beam exaggerates the wave effects, making
37
38 interpretation of results more straightforward. The unsteady speed took the form:
39
40
41

$$42 \quad U(t) = \bar{U} + \hat{U} \sin \omega t$$

43
44
45 The mean velocities, \bar{U} , perturbation velocity amplitudes, \hat{U} , and frequencies ω
46
47 were varied.
48
49

50
51 In parallel with the experiment study, an unsteady inviscid thin-ship computer code
52
53 was developed to predict the time history of the wave-making resistance in water of
54
55 any depth. The code takes advantage of the simple formulae describing the Wigley
56
57 hull to reduce computational effort in this highly numerically-intensive calculation.
58
59
60

1
2
3 Details of the hull form and the theoretical basis of the unsteady wave resistance
4 code are given in Doctors, Day & Clelland (2010).
5
6

7
8 Figure 5a shows a typical measured speed profile from the tests, plotted against
9 non-dimensionalised time. Figure 5b shows one comparison of measured and
10 predicted time histories of wave resistance R_w (non-dimensionalised with model
11 weight W), plotted against non-dimensional distance, s/L where s is the distance
12 travelled in metres. The mean Froude number is $\bar{F}_r = \bar{U}/\sqrt{gL} = 0.3$, the amplitude
13 of oscillation of the Froude Number is $\hat{F}_r = \hat{U}/\sqrt{gL} = 0.06$, and the mean depth
14 Froude Number $\bar{F}_{rh} = 1.0$.
15
16
17
18
19
20
21
22
23
24
25

26
27 The curve marked "Expt" is the unsteady wave resistance, calculated from
28 experiment data for total resistance using a quasi-steady approximation for viscous
29 resistance, in which the instantaneous viscous resistance is estimated from the
30 instantaneous speed using a standard established relationship between steady
31 speed and steady viscous resistance. The relationship adopted is known to give
32 good predictions of steady resistance for slender ships over a wide speed range.
33
34
35
36
37
38
39

40
41 The curve marked is "US" is the computational prediction for unsteady wave
42 resistance; finally the curve marked "QS" is the predicted quasi-steady wave
43 resistance, calculated from the variation of steady wave resistance with steady
44 speed, as predicted by a conventional steady thin-ship wave-resistance code.
45
46
47
48
49

50
51 This plot illustrates some of the challenges of shallow-water oscillatory testing: the
52 oscillations in the wave resistance curve grow as the model progresses along the
53 tank. This behaviour is correctly predicted by the unsteady code, whilst the quasi-
54 steady approach, based on the steady code, yields extremely poor prediction of the
55 time history, dramatically underestimating the peaks of the resistance curve.
56
57
58
59
60

1
2
3 Figure 5c shows the root-mean-square wave resistance plotted against the
4
5 frequency parameter $\tau = U\omega/g$ (where ω is the oscillation frequency in rad/s). This
6
7 parameter indicates the ratio between the forward speed of the vessel and the
8
9 phase speed of the waves generated by the oscillation (in deep water). The value at
10
11 $\tau = 0$ indicates the corresponding steady-speed value. It can be seen that over
12
13 much of this range, the unsteady value is substantially higher than the steady-speed
14
15 value. The substantial “hump” in the graph around $\tau = 0.16$, is well predicted by the
16
17 theory.
18
19
20
21

22 In general, good agreement was found at low mean speeds and oscillation
23
24 frequencies between the unsteady shallow-water wave-resistance computations and
25
26 the values derived from tank tests. It can thus be inferred that the effects of shallow
27
28 water on wave-making resistance at unsteady speed can be correctly predicted
29
30 using the computational approach in these conditions. The agreement also gives
31
32 some reassurance that the tank tests are correctly reproducing the wave conditions.
33
34
35

36 Since the tank-derived values of wave resistance rely on the quasi-steady
37
38 approximation to frictional resistance, it can also be inferred that in these conditions
39
40 the viscous resistance is well predicted by this approximation. In contrast, there is
41
42 very poor agreement between tank-derived values for unsteady wave resistance
43
44 and predicted quasi-steady approximation for wave resistance.
45
46
47

48 However subsequent tests at higher mean speeds and with higher values of the
49
50 frequency parameter, closer to those experienced in rowing and/or kayaking races,
51
52 did not show such good agreement. The data for Figure 6 was obtained with
53
54 $\bar{F} = 0.5$, $\hat{F} = 0.1$ and $F_{rh} = 1.0$; it can be seen that the trends are poorly predicted
55
56 for $\tau > 0.7$. Much higher values than this are found in rowing races; for example the
57
58 data shown in Figure 1 corresponds to $\bar{F} = 0.498$, $\hat{F} = 0.09 (+)$, $\hat{F} = 0.15 (-)$,
59
60

1
2
3 and $\tau = 1.86$. At these higher frequencies, the measured resistance is found to be
4
5 substantially greater than that predicted using the computational approach,
6
7 suggesting that the approach is breaking down in conditions relevant to rowing.
8
9

10
11 However, the unsteady wave-resistance calculation makes no assumptions about
12
13 speed or frequency except a common linearization that wave steepness is small.
14
15 Hence, the approach should in principle also behave well at higher speeds and
16
17 frequencies, unless wave behaviour changes dramatically in some way. This could
18
19 result from wave-breaking; however, video recordings show no evidence of this.
20
21

22
23 A more likely corollary is that the quasi-steady approximation for the viscous
24
25 resistance is failing in these conditions, and that viscous resistance increases
26
27 substantially in these higher speed and frequency conditions. One possible
28
29 contributor to this is the influence of acceleration on turbulence in the boundary layer
30
31 and in particular on the transition between laminar and turbulent flow. Predicting the
32
33 location of the laminar- turbulent transition from first principles is a hugely
34
35 challenging problem in ship resistance prediction even in steady flow; in unsteady
36
37 flows of the type of interest here there is virtually no information available.
38
39

40
41 The location of laminar-turbulent transition is known to be of great practical
42
43 relevance in hull design optimisation; designing bow shapes to delay transition is a
44
45 key strategy for resistance reduction in yachts, and has been extensively
46
47 investigated by America's Cup technical teams. A preliminary indication of the
48
49 importance of the location of laminar-turbulent transition in the present context was
50
51 given by steady speed tests with transition "forced" at different locations by a girth-
52
53 wise line of small studs fitted to the surface of the hull. For the single scull used
54
55 here, the steady resistance at 4.0m/s was found to be around 1.5% higher with
56
57 studs located 400mm from the bow compared to a case with studs at 600mm.
58
59
60

1
2
3 The second phase of the study thus focussed on unsteady effects on laminar-
4
5 turbulent transition. As well as providing insight into unsteady effects on viscous
6
7 flow, transition provides a useful metric for the comparison of laboratory and field-
8
9 trial data for validation purposes. Total hull resistance would be the ideal choice, but
10
11 is impractical due to the challenges associated with the measurement of hull
12
13 resistance in the field with suitable accuracy.
14
15

16 17 18 **4 Field Measurement of Viscous Flow** 19

20 A series of field trials was carried out with the twin objectives of establishing realistic
21
22 speed profiles for reproduction in the tank, and providing field measurements
23
24 against which the test-tank data could be validated to demonstrate that realistic
25
26 viscous flow can be created in the absence of the athlete.
27
28

29
30 A single scull was chosen for these trials since it could be tested at full-scale in the
31
32 tank, hence avoiding scaling issues for this preliminary study. Three series of field
33
34 trials were carried out, in varying conditions and locations, allowing progressive
35
36 refinement of the systems, and also allowing the rower to become accustomed to
37
38 the reduced stability of the hull resulting from the installed equipment.
39
40

41
42 The scull was fitted with conventional hot-film anemometry gauges (Dantec
43
44 Dynamics Ltd, Bristol, UK) in a number of different locations. In the early sets of
45
46 tests several gauges were set up to identify suitable locations on the hull (see
47
48 Figure 7a); as runs progressed, forward gauges were removed to allow undisturbed
49
50 flow to gauges further aft. In the final set of tests one gauge was located on each
51
52 side in the best positions identified order to ensure no interference between the
53
54 gauges.
55
56

57
58 Motions were recorded using an integrated system designed for logging race-car
59
60 data (VBox 3i, Racelogic, Buckingham, UK); this comprises GPS to capture mean

1
2
3 speed, accelerometers to obtain surge and pitch motions, and a portable data logger
4 including analogue inputs used here to gather the hot-film data. The data logger and
5 hot-film amplifiers were mounted in a waterproof box aft of the foot stretcher, as
6 shown in Figure 7b.
7
8
9

10
11
12 Several runs were made during each set of trials; each run included some “cruising”
13 strokes, some “racing” strokes, and also a “coast-down” period, in which the scull
14 decelerates smoothly in a natural manner. A sample of measured motion data from
15 the field trials is shown in Figure 8.
16
17
18
19
20

21
22 The present study focusses on the flow behaviour at the faster stroke rate; a
23 representative cycle was chosen with maximum speed of 4.4m/s. The time-history
24 from the trials motion was then used to create an input file for the sub-carriage drive
25 system. The resulting time history of position is shown in Figure 9.
26
27
28
29
30

31 32 33 **5 Towing-tank measurement of viscous flow**

34
35 The second set of tank tests also focussed on the measurement of turbulence near
36 the bow of a full-scale single scull. The scull used was similar, but not identical, to
37 that used in the field trials. Hot-film gauges were applied in positions similar to those
38 used in the final set of field trials, at 400mm and 600mm aft of the bow.
39
40
41
42

43
44 The hot-film signal can be characterised as consisting of four main components: a
45 DC signal that varies non-linearly with speed; a DC signal that is higher for turbulent
46 flow than for laminar flow; an AC signal representing flow turbulence, and
47 intermittency when the flow is sometimes laminar and sometimes turbulent.
48
49
50
51
52

53
54 A series of runs were first carried out at steady speed to test the hot-film
55 measurements. The data was filtered with a low-pass digital filter with 20Hz cut-off
56 to remove electrical noise. Figure 10 shows a time history of a typical run.
57
58
59
60

1
2
3 The non-linear variation of hot-film signal with speed can be seen between 1-3s.
4
5 Jumps of around 0.5V in the hot-film signals can be observed at just after 3s for the
6
7 aft gauge and after 4s for the forward gauge, indicating laminar-turbulent transition.
8
9
10 Once the speed reaches a constant value, the signal level drops as the flow re-
11
12 laminarises; occasional bursts of turbulence are still observed on the aft gauge
13
14 where the Reynolds Number is higher. This plot indicates the influence of even
15
16 simple and smooth acceleration patterns on transition.
17

18
19 In order to confirm the impact of turbulent flow on output signal, one run was carried
20
21 out with a small wire attached forward of the forward gauge in order to force
22
23 transition. The jump in signal was similar to that observed with natural transition.
24
25

26
27 A series of oscillatory runs was then carried out reproducing the field-trial motions.
28
29 Figure 11 shows data from a run at mean speed comparable to the field trials. This
30
31 data is filtered, but otherwise unprocessed; zero offsets have not been removed. It
32
33 can be seen that the signal displays variations due to both the speed changes, and
34
35 transition from laminar to turbulent flow.
36
37

38
39 An attempt was then made to separate the effect on output signal of speed variation
40
41 from the effect of transition. Using the data from constant-speed runs, calibration
42
43 curves for each of the hot-film gauges were derived, and used with the
44
45 instantaneous speed data to generate a quasi-steady approximation to the speed-
46
47 related component of the signal. This quasi-steady approximation was subtracted
48
49 from the total signal.
50

51
52 The remainder can be regarded as an estimate of the unsteady component of the
53
54 signal – i.e. the part related to flow acceleration. The impact of this process is shown
55
56 in Figure 12 along with non-dimensional acceleration data indicating the phase of
57
58 the signal. It can be seen that the estimated unsteady components are close to zero
59
60

1
2
3 when the acceleration is small, indicating that the decomposition of signal into quasi-
4 steady and unsteady components has been largely successful.
5
6

7
8 The results show a marked relationship between acceleration and turbulence: the
9 unsteady component clearly peaks on both gauges at peak deceleration, indicating
10 that rapid deceleration is triggering transition; as might be expected, the turbulence
11 lasts longer on the aft gauge at higher Reynolds Number. A secondary peak
12 appears regularly on the aft gauge near the secondary local minimum of the
13 acceleration. The pattern of the unsteady component, though complex in form,
14 appears strongly periodic in nature, with features repeating over several cycles. The
15 increased levels of turbulence suggest that viscous resistance will be higher than in
16 a comparable steady-flow situation. It was found that this unsteady component was
17 relatively insensitive to the mean speed; reducing the mean speed to 3.0m/s was
18 found to have little impact on the shape of the curve.
19
20
21
22
23
24
25
26
27
28
29
30
31
32

33 Since the emphasis for the validation is on the unsteadiness of the flow, it seems
34 reasonable to adopt this unsteady component as a metric to compare the influence
35 of acceleration on viscous flow in tank and field trials.
36
37
38
39
40

41 **6 Comparison of unsteady flow in laboratory and field trial data**

42 A similar approach was taken to analyse the trials data. Calibration curves were
43 estimated from coast-down data, and used to calculate the unsteady component of
44 the hot-film output for comparison with tank data.
45
46
47
48
49

50 Several sections of trials data were identified as similar to the tank data in terms of
51 velocity and acceleration. Key comparisons for one section of field data are shown
52 in Table 1; Figure 13 shows the corresponding perturbation velocity and
53 acceleration, normalised with respect to their maximum absolute values. The time
54 scales of both signals are normalised with respect to stroke periods to aid
55
56
57
58
59
60

1
2
3 comparison. It can be seen that the field-trial and laboratory velocity signals are very
4
5 similar, but some small details of acceleration differ slightly.
6
7

8
9 Figure 14 shows the results for the gauges located 600mm from the bow for these
10
11 sections of the time histories. The field-trial hot-film data has been offset for clarity
12
13 and also scaled to account for differences in amplifier settings between field and
14
15 tank tests; this does not affect the validity of the comparison since the focus here is
16
17 on the variation of signal with time rather than the absolute magnitude of the signal.
18
19

20
21 It can be seen that the key features of the signal are largely comparable between
22
23 laboratory and field data. The field-trials data exhibits more variability than the data
24
25 from the laboratory. This could be expected for three reasons: background
26
27 turbulence levels are likely to be higher in the field trials; stroke-to-stroke variations
28
29 are greater; finally the impact of athlete movement on heave and pitch will be
30
31 variable in the field trials.
32
33

34
35 Both data sets show a large periodic double peak suggesting onset of turbulent flow
36
37 at peak deceleration (e.g. $t/T \approx 2.125 - 2.250$). The relative magnitude of the two
38
39 peaks varies rather more in the trials data than in the laboratory data. Both data sets
40
41 also show a second smaller set of periodic double peaks which correspond to a
42
43 local minimum acceleration (e.g. $t/T \approx 0.75$); this peaks are slightly more variable
44
45 in the trials data, failing to appear in the second stroke shown. The only periodic
46
47 feature in the trials data which does not appear in the laboratory data is a third peak
48
49 which appears to occur near the maximum positive acceleration ((e.g. $t/T \approx 0.5$)).
50
51 Examination of motion data does not suggest any particular cause for this.
52
53

54
55 Nonetheless the general character of the signals is unquestionably similar in most
56
57 respects. Thus it is proposed that the testing methodology correctly recreates the
58
59 complex mechanisms of unsteady viscous flow in the towing tank.
60

7 Discussion and Conclusions

The study has described the development of a test rig for generating realistic oscillatory speed profiles for a test hull in a towing tank. The test rig has been used to identify the presence of some complex unsteady shallow-water wave-resistance phenomena. The mean unsteady wave resistance is shown to be considerably higher than the comparable steady-state value in some cases.

The computational study showed that at low speed and low frequency the unsteady resistance for a benchmark model hull is well predicted by a combination of unsteady wave-resistance and quasi-steady viscous-resistance models. The good agreement also gives reassurance that shallow-water unsteady wave resistance is correctly represented in the tank tests.

However, results also indicate that the quasi-steady approximation for viscous forces is not valid at higher speeds and frequencies, and that unsteady viscous resistance is higher than predicted by the quasi-steady approximation. This suggests that accurate computational prediction of the unsteady total resistance at these speed and frequencies presents substantial challenges.

The test rig has been used to identify the impact of unsteady effects on laminar-turbulent transition in both laboratory and field-trial conditions. In both cases turbulence is shown to be strongly related to acceleration through the stroke cycle. Comparison of tank test results with field-trial measurements show that the unsteady viscous flow phenomena identified in the real-world measurements are also present in the tank. Hence it can be concluded that the rig generates plausible unsteady viscous flow phenomena in the test tank, and thus the tank tests could reliably be used to investigate improved designs.

The use of a test rig which can replicate the real-world hydrodynamics of rowing shells or canoes/kayaks, opens the door to a number of opportunities for

1
2
3 performance improvements. The approach can be used to assess designs directly,
4
5 or to validate CFD calculations. Designs intended to reduce resistance can be
6
7 evaluated in realistic conditions in a controllable and repeatable environment,
8
9 allowing measurement of the flow characteristics and the dynamic forces.
10

11
12 A study of the effect of the unsteady speed profile on the unsteady resistance for
13
14 realistic rowing conditions is planned. A more generic study utilising a thin flat plate
15
16 to examine in detail the impact of unsteady speed on viscous resistance is also
17
18 planned. Finally it is intended to generalise the computer code to allow prediction of
19
20 resistance of any slender hull form.
21
22

23
24 However there are still two key questions to be addressed. In this study a single
25
26 scull was used because the size and speed of the single allowed full-scale tests to
27
28 be carried out within the limitations of the test tank. Even so, only a small number of
29
30 oscillation cycles was possible at full speed. Canoes and kayaks would be
31
32 amenable to testing in this manner with similar limitations. However in order to test
33
34 rowing pairs, fours or eights, scale models would be required. Froude similarity
35
36 would then lead to lower model-scale testing speed, and higher model-scale
37
38 frequency, and hence more oscillations in the scope of the tank, but further
39
40 validation would be desirable in order to understand more completely the scaling of
41
42 the unsteady viscous effects.
43
44

45
46 Finally, in order to complete the accuracy of the modelling, it would be also desirable
47
48 to build a more sophisticated mechanism to replicate the complete six-degree-of-
49
50 freedom motions precisely. It is likely that heave and pitch will be the dominant
51
52 modes of motion in rowing applications in which power is applied in a symmetrical
53
54 fashion, whilst roll and yaw motions will also be important in canoe/kayak
55
56 applications due to the asymmetry of the power application.
57
58
59
60

References

Berton, M., Alessandrini, B., Barré, S. and Kobus, J.M. (2007). Verification and validation in computational fluid dynamics: application to both steady and unsteady rowing boats numerical simulations. *Proc. 16th ISOPE Conference*, 3, 2006-2011, Lisbon, Portugal.

Bugalski, T. J. (2009). Development of the New Line of Sprint Canoes for the Olympic Games. *10th International Conference on Fast Sea Transportation (FAST 2009)*, 1039-1049, Athens, Greece.

Doctors, L.J., Day, A.H. and Clelland, D. (2010). Resistance of a Ship Undergoing Oscillatory Motion. *J. Ship Research*, 54, No 2, 120-132.

Faltinsen, O. M. (2005). *Hydrodynamics of High-Speed Marine Vehicles*. Cambridge: Cambridge University Press.

Formaggia, L., Miglio, E., Mola, A. and Parolini, N. (2008). Fluid–structure interaction problems in free surface flows: Application to boat dynamics. *International Journal for Numerical Methods in Fluids*, 56, 965–978.

Formaggia, L., Miglio, E., Mola, A. and Montano, A. (2009). A model for the dynamics of rowing boats. *International Journal for Numerical Methods in Fluids*, 61, 119–143.

Kleshnev V. (2002). *Rowing Biomechanics Newsletter*, 2, No 6.

Lazauskas, L. (1998). Rowing Shell Drag Comparisons. Technical report L9701, Department of Mathematics, University of Adelaide. Retrieved from <http://www.cyberiad.net/library/rowing/real/realrow.htm>

1
2
3 Lazauskas, L. & Tuck, E.O. (1996). Low Drag Racing Kayaks. Technical report
4
5 Department of Mathematics, University of Adelaide. Retrieved from
6
7
8 <http://www.cyberiad.net/library/kayaks/racing/racing.htm>
9

10
11 Lazauskas, L., & Winters, J. (1997) Hydrodynamic drag of some small sprint kayaks.
12
13 Technical report Department of Mathematics, University of Adelaide. Retrieved from
14
15 <http://www.cyberiad.net/library/kayaks/jwsprint/jwsprint.htm>
16

17
18 Scragg, Carl A. & Nelson, Bruce D. (1993). The Design of an Eight-Oared Rowing
19
20 Shell. *Marine Technology*, 30, No. 2, 84-99.
21

22
23 Tuck, E.O. & Lazauskas, L., (1996). Low drag rowing shells *Proc. 3rd Conference*
24
25 *on Mathematics and Computers in Sport*, 17-34. Bond University, Queensland,
26
27 Australia,
28

29
30 Wellicome J. F. (1967). Report on Resistance Experiments Carried out on Three
31
32 Racing Shells. National Physical Laboratory Ship T.M.184.
33
34
35
36
37
38
39
40
41
42
43
44
45
46
47
48
49
50
51
52
53
54
55
56
57
58
59
60

Table 1 Velocity and Acceleration parameters for chosen comparison data

Parameter	Laboratory	Field trial	Difference (%)
Mean Velocity (m/s)	4.00	4.16	4
Peak unsteady positive perturbation velocity (m/s)	0.84	0.87	4
Peak unsteady negative perturbation velocity (m/s)	-1.33	-1.37	3
Peak negative acceleration (m/s ²)	-6.85	-6.11	-11
Peak positive acceleration (m/s ²)	3.65	-3.87	6
Stroke Period (s)	1.83	2.03	11
Stroke Rate (1/min)	32.8	29.6	-9

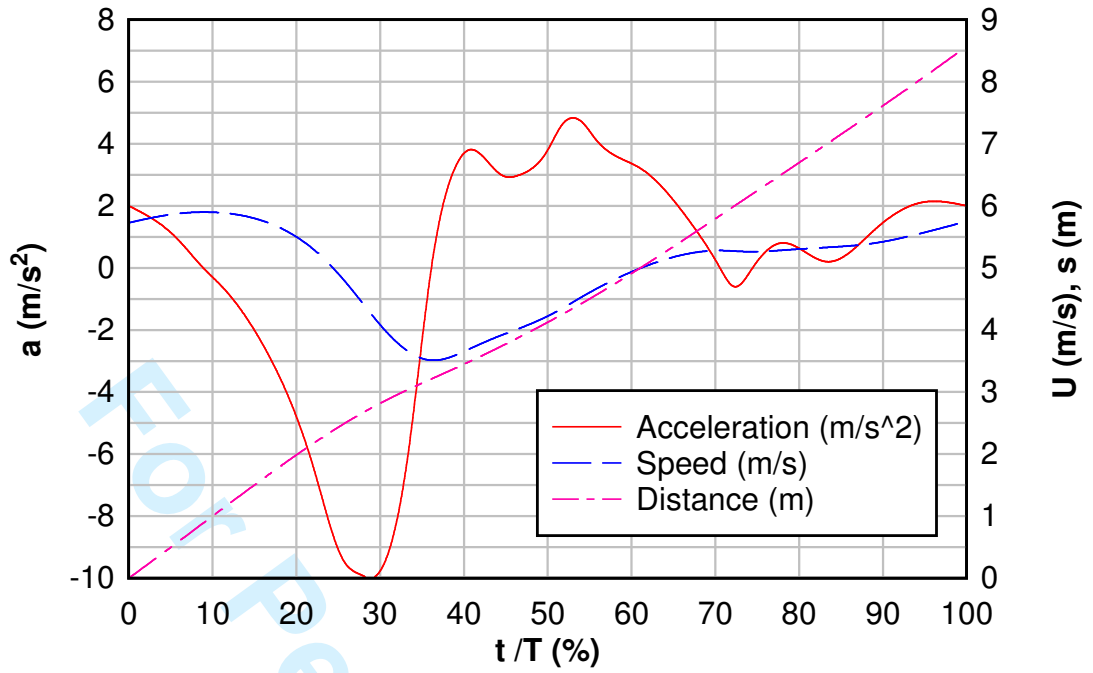


Figure 1: Measured surge acceleration and resulting speed and distance (acceleration re-plotted from Kleshnev (2002))

Free Review Only

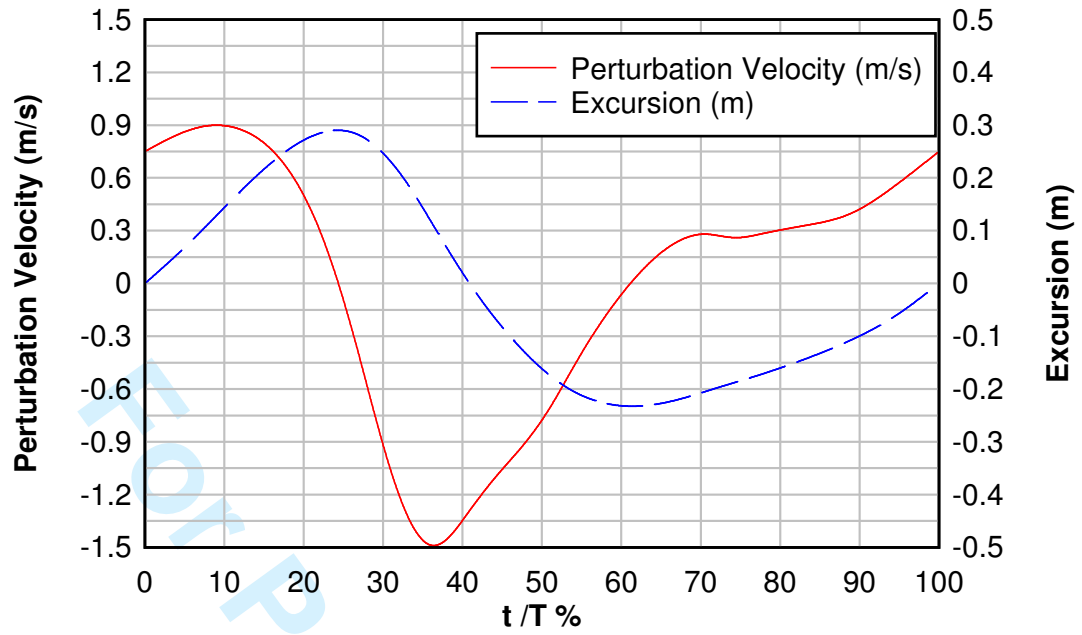


Figure 2 Perturbation velocity and excursion for full-scale rowing pair

1
2
3
4
5
6
7
8
9
10
11
12
13
14
15
16
17
18
19
20
21
22
23
24
25
26
27
28
29
30
31
32
33
34
35
36
37
38
39
40
41
42
43
44
45
46
47
48
49
50
51
52
53
54
55
56
57
58
59
60

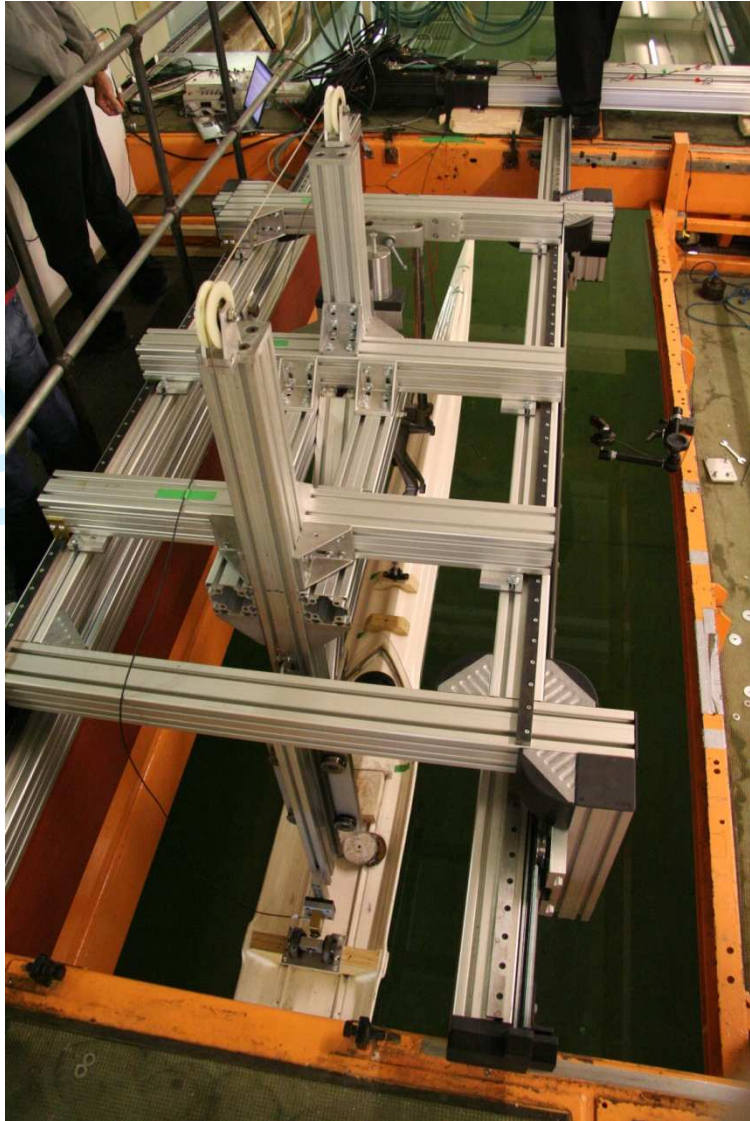


Figure 3 Sub-carriage set up with single scull

1
2
3
4
5
6
7
8
9
10
11
12
13
14
15
16
17
18
19
20
21
22
23
24
25
26
27
28
29
30
31
32
33
34
35
36
37
38
39
40
41
42
43
44
45
46
47
48
49
50
51
52
53
54
55
56
57
58
59
60

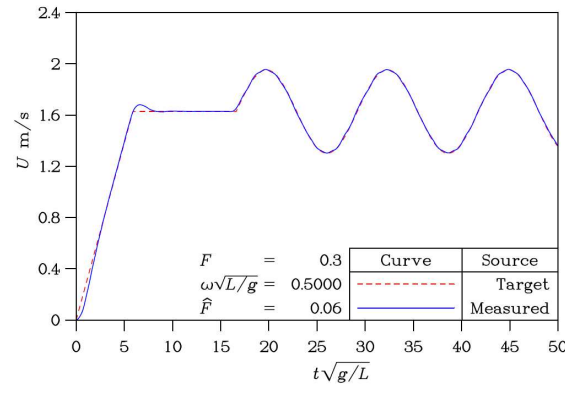


Figure 4 Shallow water testing of Wigley Hull

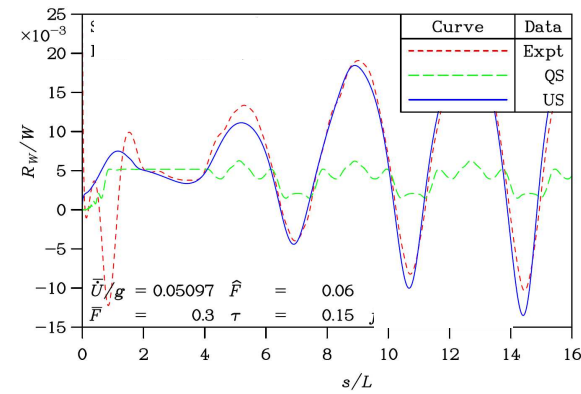
Review Only

1
2
3
4
5
6
7
8
9
10
11
12
13
14
15
16
17
18
19
20
21
22
23
24
25
26
27
28
29
30
31
32
33
34
35
36
37
38
39
40
41
42
43
44
45
46
47
48
49
50
51
52
53
54
55
56
57
58
59
60

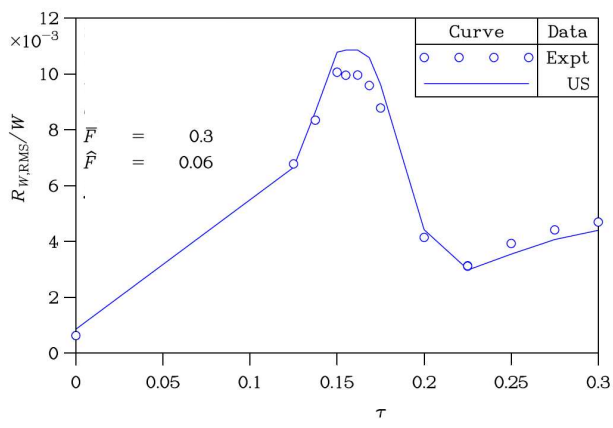
a) typical
speed
profile



b) measured
and
predicted
wave
resistance



c) measured
and
predicted
root-mean-square
wave
resistance



1
2
3
4
5
6
7
8
9
10
11
12
13
14
15
16
17
18
19
20
21
22
23
24
25
26
27
28
29
30
31
32
33
34
35
36
37
38
39
40
41
42
43
44
45
46
47
48
49
50
51
52
53
54
55
56
57
58
59
60

Figure 5 Selected Results for benchmark tests: low speed & low frequency

For Peer Review Only

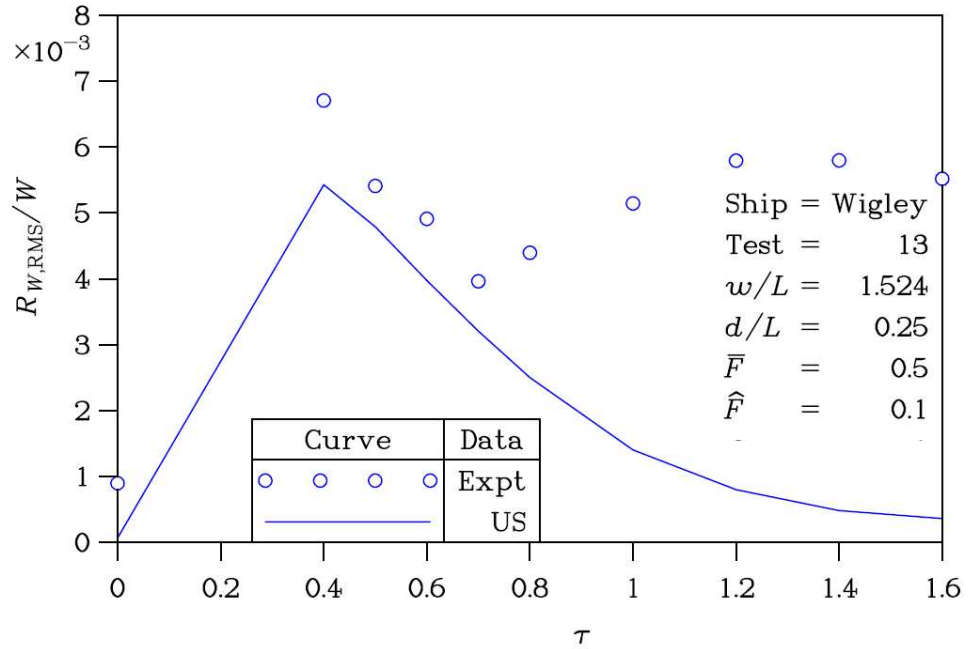


Figure 6 Root-mean-square (RMS) wave resistance for Wigley hull at moderate speed and frequency

1
2
3
4
5
6
7
8
9
10
11
12
13
14
15
16
17
18
19
20
21
22
23
24
25
26
27
28
29
30
31
32
33
34
35
36
37
38
39
40
41
42
43
44
45
46
47
48
49
50
51
52
53
54
55
56
57
58
59
60

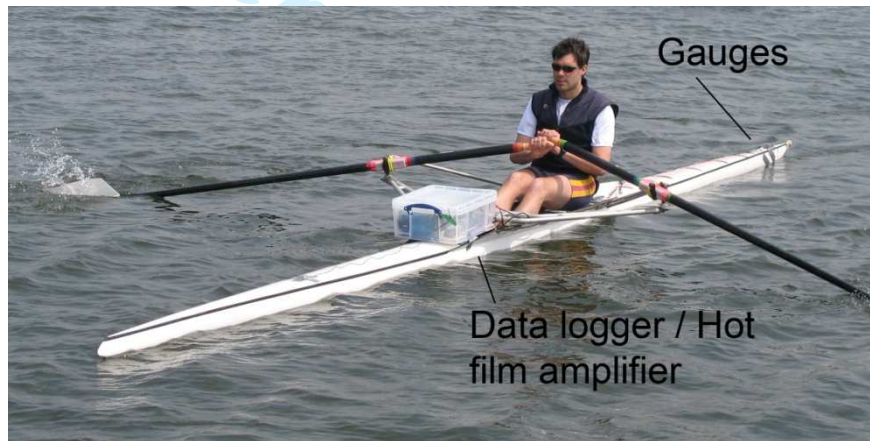
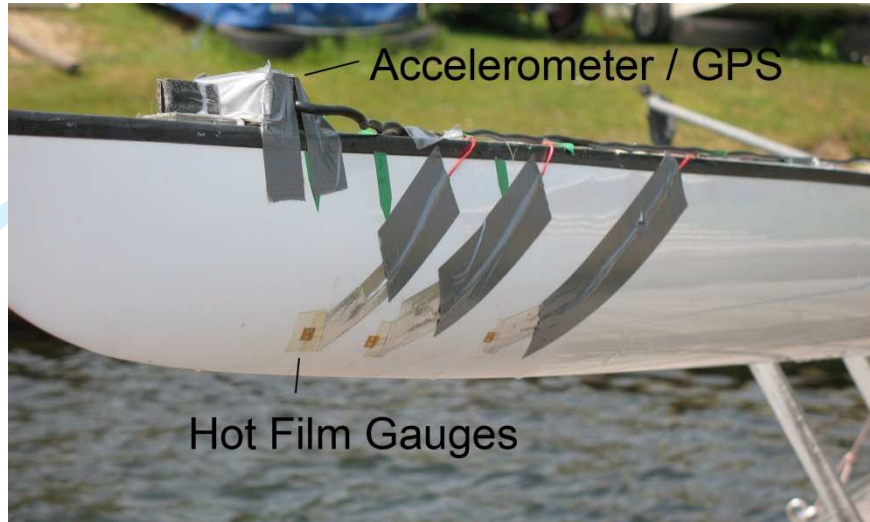


Figure 7 Instrumented single scull

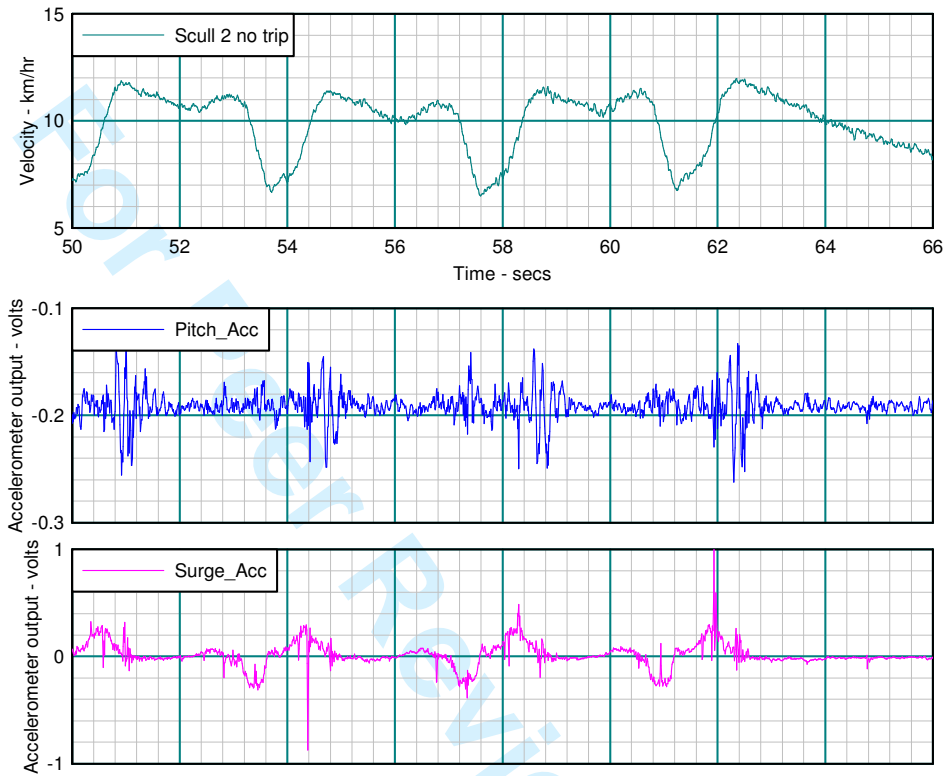


Figure 8 Typical results from field trial motion measurements

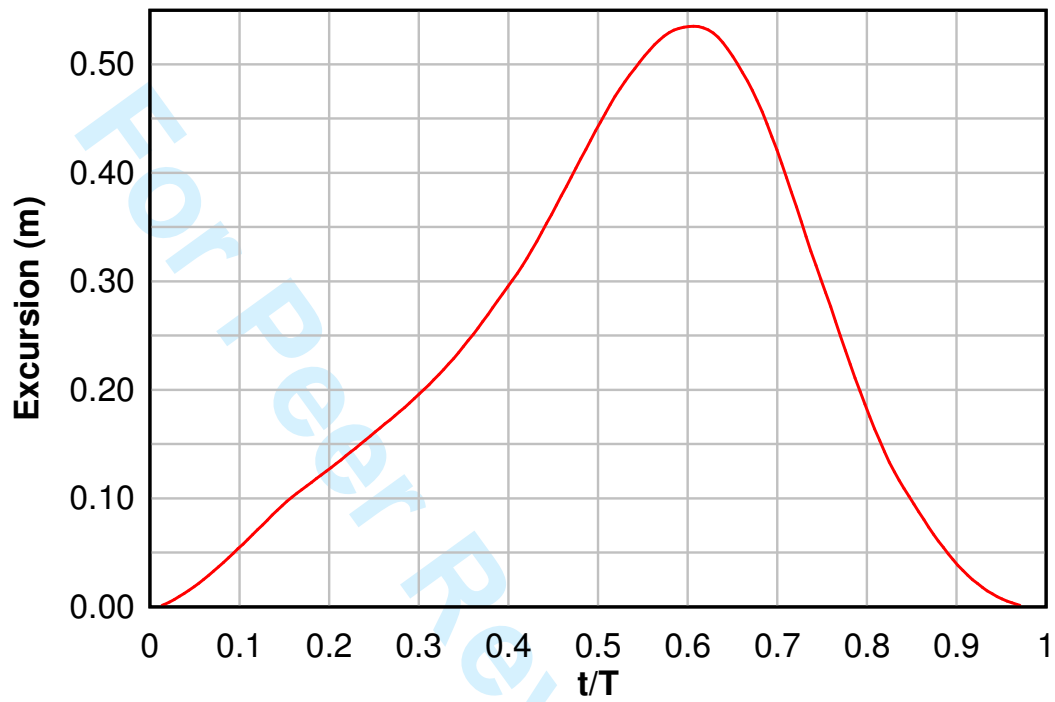


Figure 9 Carriage excursion data derived from field trials

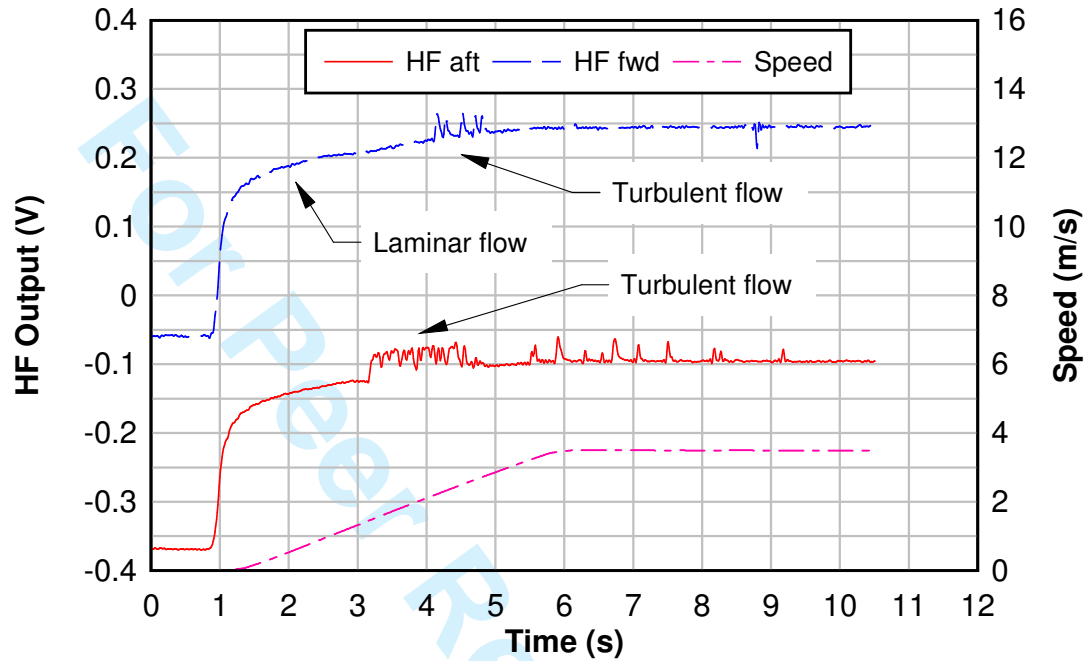


Figure 10 Typical time history of hot-film output in steady-speed tank test

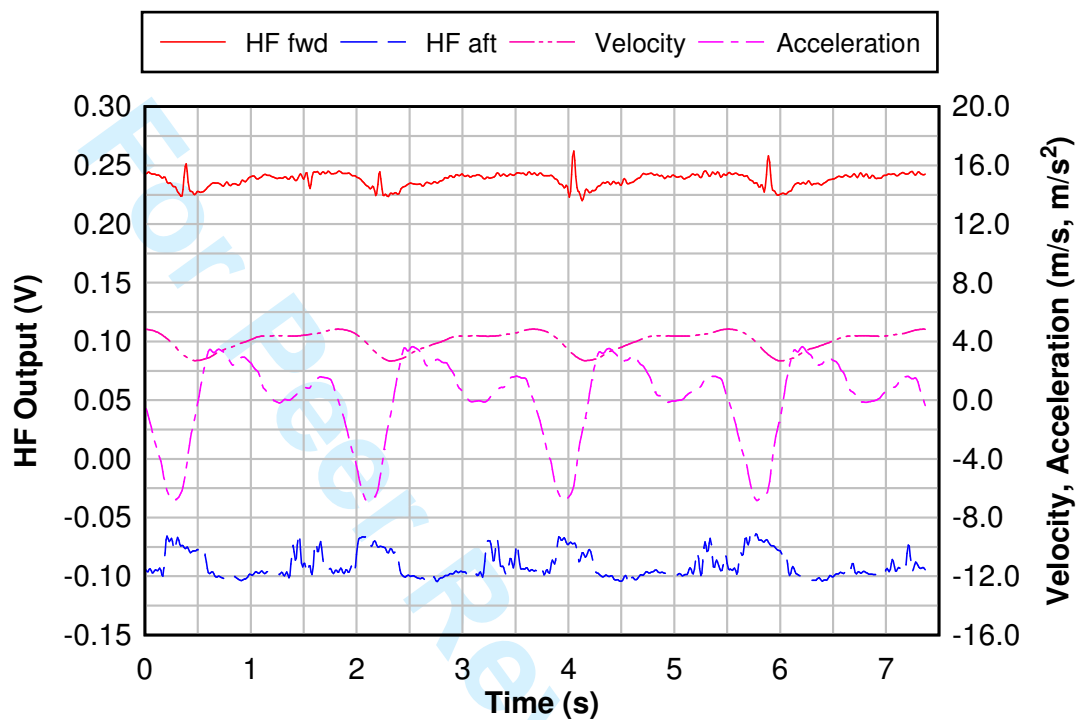


Figure 11 Typical run: Fast rowing pattern, with mean speed = 4.0m/s

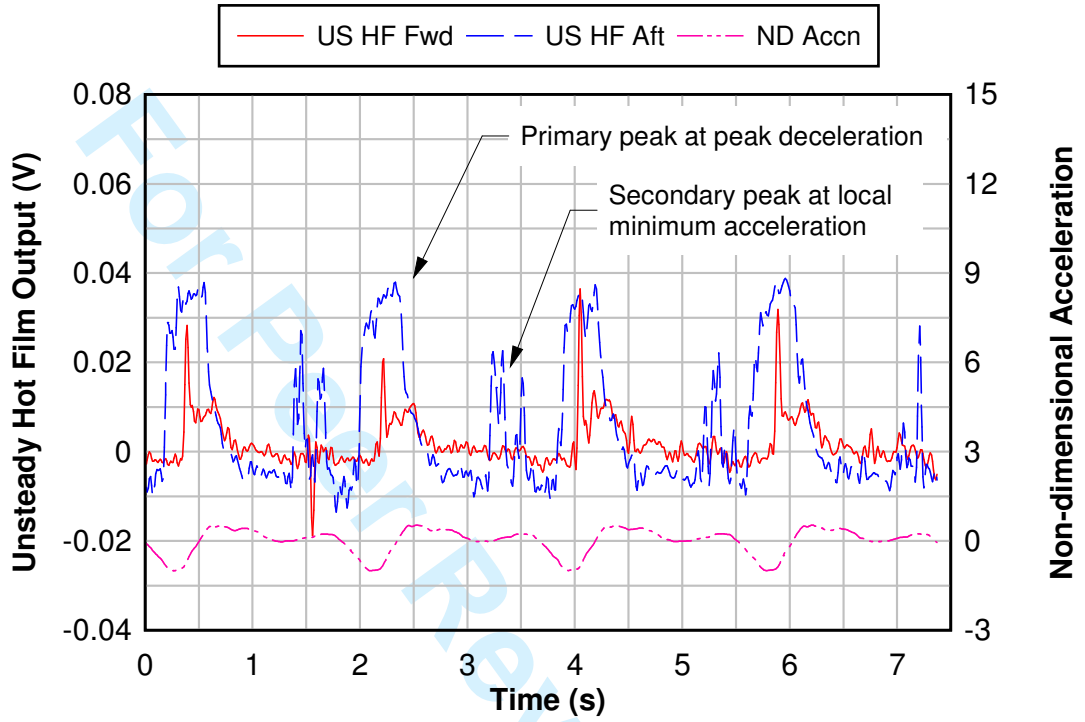


Figure 12 Unsteady component: Fast rowing pattern, mean speed = 4.0m/s

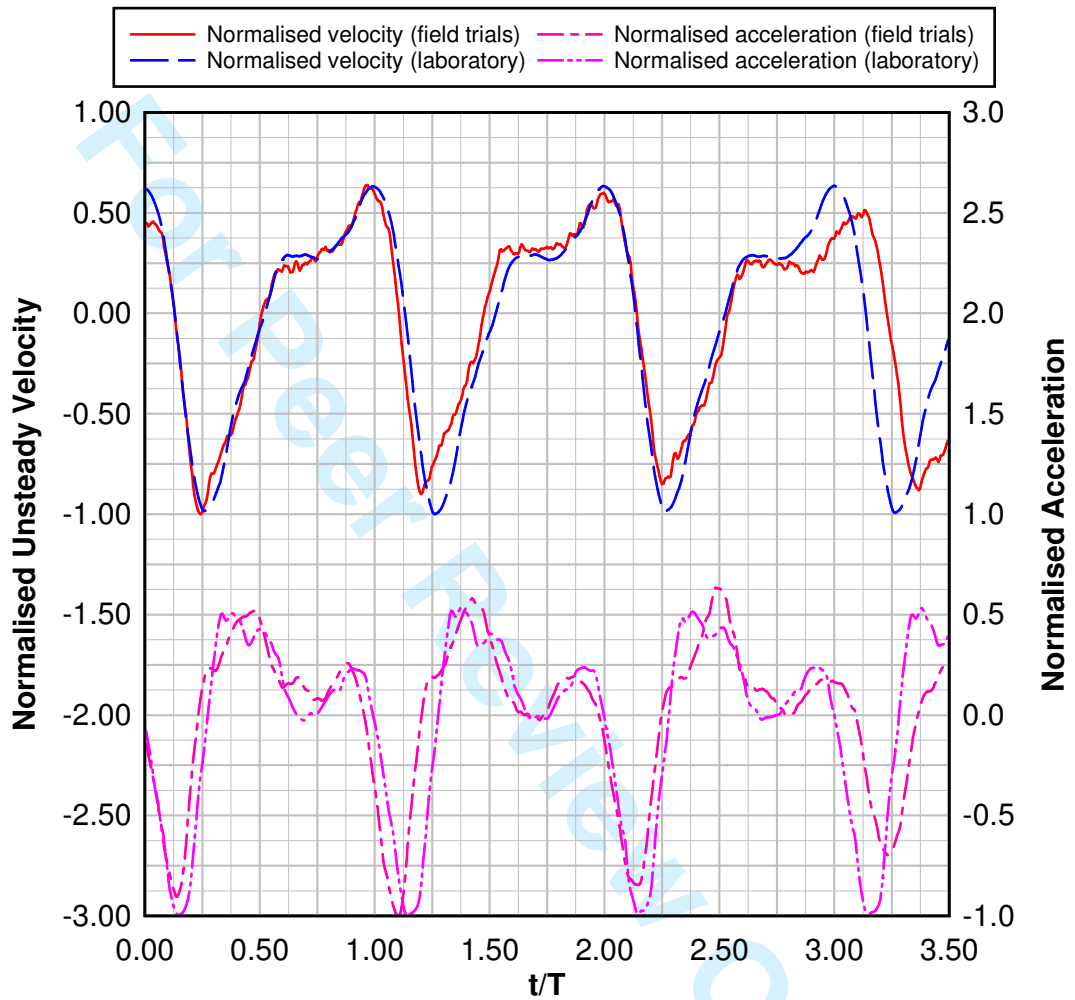


Figure 13 Comparison of velocity & acceleration data between field and tank for chosen section